RSC Advances

PAPER

View Article Online
View Journal | View Issue

Cite this: *RSC Adv.*, 2022, **12**, 15098

Monoammonium salts of multiprotic acids as dopants for proton-conductive hydrogel membranes: the effects of anions

Kainan Niu, Jie Luo, Qing Yang, Caihong Wang, Shuai Tan and Yong Wu *

Monoammonium salts of diprotic acid (NH_4HSO_4) and triprotic acid ($NH_4H_2PO_4$), whose cations and anions are both potential proton carriers, were employed as dopants for proton-conductive hydrogel membranes to explore the effects of anions on thermal, mechanical, and electrochemical performance. Robust hydrogel membranes were obtained by radical copolymerization of acrylamide and ethylene glycol dimethacrylate dissolved in aqueous solutions of NH_4HSO_4 and $NH_4H_2PO_4$. By virtue of the protonated ammonium cation, the ionic conductivities of the hydrogels doped with NH_4HSO_4 and $NH_4H_2PO_4$ were superior to those doped with the corresponding inorganic acids (H_2SO_4 and H_3PO_4). The hydrogel doped with NH_4HSO_4 exhibited a higher ionic conductivity but lower mechanical strength and thermostability than that with $NH_4H_2PO_4$. Ionic conduction in the doped hydrogels was dominated by the vehicle mechanism and NH_4HSO_4 resulted in lower activation energy for the conduction than $NH_4H_2PO_4$. In addition, the fuel cell performances of the hydrogel membranes at room temperature were evaluated.

Received 23rd February 2022
Accepted 11th May 2022

DOI: 10.1039/d2ra01208a

rsc.li/rsc-advances

1. Introduction

Hydrogels, which are a three-dimensional network of hydrophilic polymers absorbing large quantities of aqueous medium, have been used as biosensors, drug delivery vectors and separating materials by virtue of the biocompatibility and water-dependent viscoelastic behavior.[1,2] By tuning the polymeric networks or the aqueous medium, ion-conductive hydrogels can be constructed for electrochemical applications such as energy storage and conversion devices.[3–6] Introduction of acid moieties to the polymeric networks rendered hydrogels with substantial proton conductivities. For example, Suzuki *et al.* prepared acid hydrogel films based on partially phosphorylated poly(vinyl alcohol)s crosslinked by glutaraldehyde and achieved a proton conductivity of 40 mS cm^{-1} at 40 °C.[7] Zygadło-Monikowska *et al.* obtained hydrogels by copolymerization of 2-acrylamido-2-methyl-propanesulfonic acid (AMPSA) and *N*,*N*′-methylene-bis-acrylamide (MBA) dissolved in water, which exhibited high conductivities but weak mechanical performance.[8] Because the acid-modified polymers were inherently rigid, few acid polymer networks satisfied the requirements of forming flexible hydrogels.[9,10]

Adding inorganic acid dopants such as H_2SO_4 and H_3PO_4 to aqueous medium was an alternative strategy to obtain proton-conductive hydrogels. Radical polymerization of acrylamide (AM) as monomer and MBA as cross-linking agent in aqueous H_2SO_4 or H_3PO_4 solution gave acid hydrogels whose proton conductivities reached up to 10 mS cm^{-1}.[11,12] We prepared H_2SO_4-doped polyacrylamide (PAM) hydrogels using divinylbenzene (DVB) as cross-linking agent and promoted the conductivity to 187 mS cm^{-1} at 30 °C.[13] Modestino *et al.* fabricated ultra-thin proton-conductive hydrogel films (thickness, <100 nm) for electrocatalyst interfaces by submerging thermally crosslinked poly(acrylic acid)–poly(vinyl alcohol) into H_2SO_4 solution.[14] Despite the simplicity, dopants other than inorganic acids have hardly been employed to prepare proton-conductive hydrogels. Ammonium slats, which were regarded as good proton donors, have ever been utilized to dope solid poly(vinyl alcohol) and poly(ethylene oxide) for proton conduction.[15–17] Owing to the exchangeable protons available in both the cation and anions, monoammonium salts of multiprotic acids are expected to be efficient dopants for promoting conductivity of hydrogels.

The aim of present study is to evaluate the potential use of monoammonium salts of multiprotic acids as dopants to construct proton-conductive hydrogel membranes for fuel cell applications, considering the effects of acid anions. Aqueous solutions of ammonium hydrogen sulfate (NH_4HSO_4) and dihydrogen phosphate ($NH_4H_2PO_4$) were converted into PAM hydrogel membranes by radical polymerization. Ethylene glycol dimethacrylate (EGDMA) instead of MBA or DVB was employed as cross-linking agent because it had stronger gelation ability in the salt solutions and favored the structural uniformity of PAM hydrogels.[18] Impact of the acid anions on mechanical performance of the obtained hydrogels were determined by

School of Chemical Engineering, Sichuan University, No. 24 South Section 1, Yihuan Road, Chengdu 610065, China. E-mail: wuyong@scu.edu.cn

rheological, tensile, and compressive tests. Morphology of the PAM networks were observed using a scanning electron microscope (SEM) and ionic conductivities of the doped hydrogels were characterized by electrochemical impendence spectroscopy (EIS) measurements. Moreover, fuel cells were fabricated from the hydrogel membranes doped with NH_4HSO_4 and $NH_4H_2PO_4$ to evaluate the electrochemical performance under practical working conditions.

2. Experimental

2.1. Materials

AM, NH_4HSO_4 and $NH_4H_2PO_4$ were supplied from Greagent. EGDMA and 1-hydroxycyclohexylphenylketone (HCHPK) were obtained from Acros. Gas diffusion electrodes loaded with catalyst 0.5 mg Pt cm^{-2} were purchased from Suzhou YiLong-Sheng (thickness, 285 μm; pressure drop, >2.5 mm H_2O). Deionized water was used in all experiments.

2.2. Preparation of the hydrogel membranes

Hydrogel composition in this work has been optimized to balance ionic conductivities and mechanical strengths. AM (4.2 mol L^{-1}), EGDMA (0.05 mol L^{-1}), HCHPK (0.005 mol L^{-1}), ammonium salt (1.1 mol L^{-1}) and water were mixed thoroughly in a sealed glass bottle by ultrasonic vibration at room temperature for 1 h to obtain a precursor. The precursor was then poured into a mold and exposed to a 365 nm UV irradiation at an intensity of 6 mW cm^{-2}. After 30 min, a transparent hydrogel membrane was formed and demolded for succeeding characterizations. HG-$AHSO_4$ and HG-AH_2PO_4 denoted the hydrogels doped with NH_4HSO_4 and $NH_4H_2PO_4$, respectively. The monoammonium salts were the only dopants loaded in the hydrogels. The synthetic route and photographs of the resultant hydrogel membranes are shown in Fig. 1.

3. Characterization

3.1. Hydrogel structures

Fourier transform infrared (FT-IR) spectra were measured by a PerkinElmer Spectrum Two Li10014 spectrometer in the range of 400–4000 cm^{-1}. HG-$AHSO_4$ and HG-AH_2PO_4 were desalted in deionized water and then freeze-dried in Sientz 10 W vacuum freeze dryer to obtain XG-$AHSO_4$ and XG-AH_2PO_4 xerogels. SEM observations of the xerogels were performed under a FEI Quanta 250 SEM running under 5 kV.

3.2. Thermal and mechanical parameters

Thermogravimetric (TG) analyses were conducted on a METTLER TOLEDO thermo gravimetric analyzer at a heating rate of 10 °C min^{-1} under an air atmosphere. Dynamic rheological analyses were performed on an Anton Paar MCR302 rheometer at 25 °C. The frequency sweep curves of cylindrical specimens (ø25 × 2 mm) were measured in a linear viscoelastic region (frequency range, 0.01–10 Hz; strain, 1%). Tensile and compressive measurements were carried out at 25 °C using an Instron 5967 electronic universal tester. The tensile tests were conducted using the dumbbell-shaped specimens (cross section: 4 × 5 mm) at a displacement rate of 20 mm min^{-1}. The compressive tests were performed using cylindrical specimens (ø14 × 17 mm) at a displacement rate of 2 mm min^{-1}.

3.3. Electrochemical parameters

Acidities (pH values) were measured by a York PHS-3C acidometer with a E-201-9 glass electrode. EIS measurements were conducted on an EG&G Princeton Application Research Versa STAT 3 workstation connecting with the PC running the electrochemical impedance software (frequency range: 1 MHz to 100 Hz; AC amplitude: 10 mV). Samples were sandwiched between two pieces of indium tin oxide (ITO) glass slides to collect impedance responses. The sample temperature was controlled by a hot-stage (WT-3000). The bulk resistance R_b (Ω) was obtained by fitting the impedance response with ZSimpWin software. Ionic conductivity σ (S cm^{-1}) was then calculated based on the space between the electrodes (d, cm) and the contact area between sample and the electrodes (A, cm^2).

$$\sigma = \frac{d}{R_b A} \quad (1)$$

3.4. Fuel cell assembly and performance

Owing to self-adhesiveness of the hydrogels, a membrane electrode assembly (MEA) was effortlessly constructed by sticking the Pt-loaded diffusion electrodes to both surfaces of a hydrogel membrane as shown in Fig. 2. The MEA was then

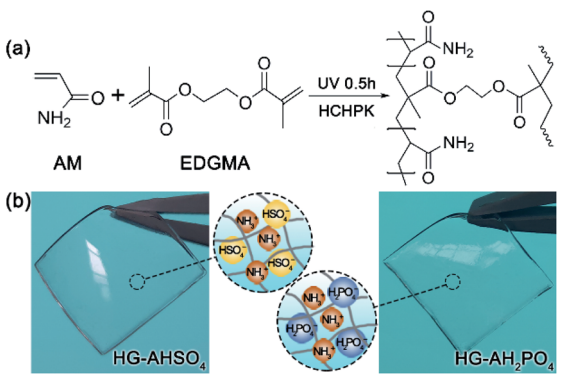

Fig. 1 (a) Synthetic route of the polymer network and (b) photographs of HG-$AHSO_4$ and HG-AH_2PO_4 membranes.

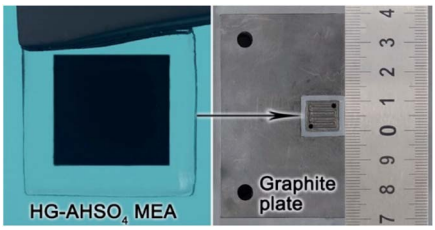

Fig. 2 Photographs of HG-$AHSO_4$ MEA and graphite plate of fuel cell.

clamped between a pair of graphite plates engraved with serpentine gas flow channels to obtain a single fuel cell with an active area of 1 cm^2. Humidified H_2 as fuel and O_2 as oxidant were continuously fed to the anode and cathode at rates of 160 and 80 mL min^{-1}, respectively. The unreacted fuel and oxidant gases were discharged without back pressure. Polarization curves of the fuel cells were collected at room temperature using a programmable DC electronic load (IT8512, ITECH).

4. Results and discussion

4.1. Architectures of the doped hydrogels

FT-IR spectra suggested that copolymerization of AM and EGDMA was successfully. As shown in Fig. 3, the bands at 1613 and 988 cm^{-1} in the spectra of HG-$AHSO_4$ and HG-AH_2PO_4 precursors were ascribed to the stretching and bending vibrations of the C=C bond, respectively. The bands disappeared in the spectra of HG-$AHSO_4$ and HG-AH_2PO_4 owing to the polymerization. The band at 1204 cm^{-1} in the spectrum of NH_4HSO_4 solution arose from the stretching vibration of the S=O bond, shifting to 1183 cm^{-1} in the spectrum of HG-$AHSO_4$ (Fig. 3a). The fact indicated that the S=O bond of the HSO_4^- anion as acceptor formed hydrogen bond with the N–H bond of amide.[19] Hydrogen bond between the $H_2PO_4^-$ anion and amide was also evidenced by the band shift of the stretching vibration of the P=O bond from 1157 cm^{-1} in the spectrum of $NH_4H_2PO_4$ solution to 1116 cm^{-1} in that of HG-AH_2PO_4 (Fig. 3b).[20]

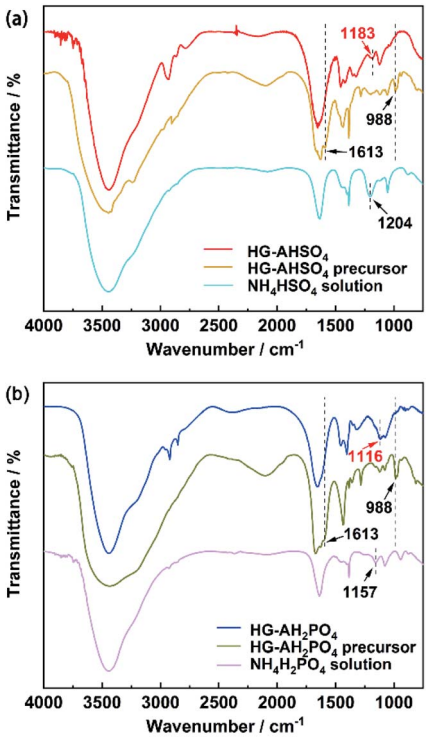

Fig. 3 FT-IR spectra of (a) HG-$AHSO_4$, HG-$AHSO_4$ precursor, NH_4HSO_4 solution and (b) HG-AH_2PO_4, HG-AH_2PO_4 precursor, $NH_4H_2PO_4$ solution.

SEM images of XG-$AHSO_4$ and XG-AH_2PO_4 revealed morphologies of PAM networks in the hydrogels doped with the ammonium salts. As shown in Fig. 4, both XG-$AHSO_4$ and XG-AH_2PO_4 exhibited a porous architecture, suggesting that EGDMA participated in the cross-linking efficiently. However, the pore size and wall thickness of XG-AH_2PO_4 were much larger than those of XG-$AHSO_4$. The difference in the morphology was supposed to arise from the different solubility of AM in the precursors. At 25 °C, the maximum dissolved amounts of AM in HG-$AHSO_4$ and HG-AH_2PO_4 precursors were measured to be 1845 and 933 g L^{-1}, respectively. During the polymerization, AM in HG-AH_2PO_4 precursor tended to precipitate so that denser walls formed as observed in PAM hydrogels prepared at low temperatures.[21] The morphology of PAM network had impacts on mechanical and electrochemical performance of the doped hydrogels as discussed later.

4.2. Effect of anion on the mechanical strengths of the hydrogels

Viscoelastic behavior of HG-$AHSO_4$ and HG-AH_2PO_4 was characterized with dynamic mechanical analysis and the resultant frequency dependent storage (G') and loss (G'') moduli are shown in Fig. 5. HG-$AHSO_4$ and HG-AH_2PO_4 exhibited essentially identical viscoelastic behavior over the measured frequency range. G' was always higher than G'' because the elastic deformation of the polymer network overwhelmed the plastic one. G' of HG-$AHSO_4$ was almost identical to that of HG-AH_2PO_4 while G'' of HG-$AHSO_4$ was slightly higher than that of HG-AH_2PO_4. The enhanced G'' of HG-$AHSO_4$ originated likely from the smaller pore size of the polymer network, which had greater hindrance to the shear deformation.[22] The moduli of HG-$AHSO_4$ and HG-AH_2PO_4 showed a weak frequency dependence and the both loss factors (tan δ) kept approximately at 0.1

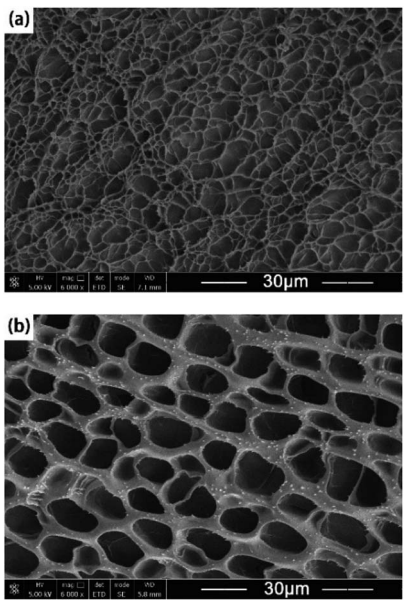

Fig. 4 Cross sectional SEM images of (a) XG-$AHSO_4$ and (b) XG-AH_2PO_4.

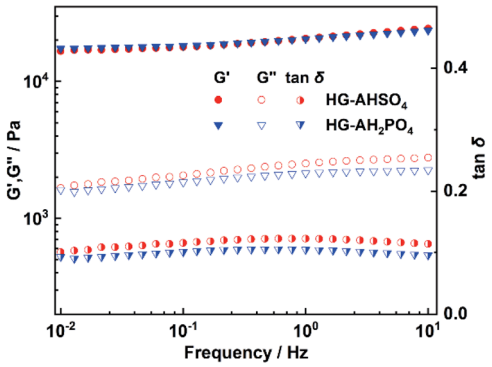

Fig. 5 Changes of G', G'', and tan δ as a function of frequency for HG-$AHSO_4$ and HG-AH_2PO_4 at 25 °C.

over the measured frequency range. The elasticity-dominated behavior of the hydrogels doped with the ammonium salts favored the application in fuel cells.

Mechanical strengths of HG-$AHSO_4$ and HG-AH_2PO_4 were determined by tensile and compressive measurements. As shown in Fig. 6a, HG-AH_2PO_4 broke at a tensile strain of 405% with a stress of 87 kPa while HG-$AHSO_4$ broke at a lower tensile strain (333%) with a reduced stress (52 kPa). The thicker walls of the network endowed HG-AH_2PO_4 with a higher strength and the larger pores of the network allowed HG-AH_2PO_4 to deform at a higher magnitude. For the same reason, the compressive stress of HG-AH_2PO_4 was higher at the same strain (Fig. 6b). At a compressive strain of 90%, the compressive stresses of HG-$AHSO_4$ and HG-AH_2PO_4 reached 1.95 and 2.38 MPa, respectively. The robust mechanical strengths of the hydrogels doped with the ammonium salts assured stable geometric shape for the fuel cell application.

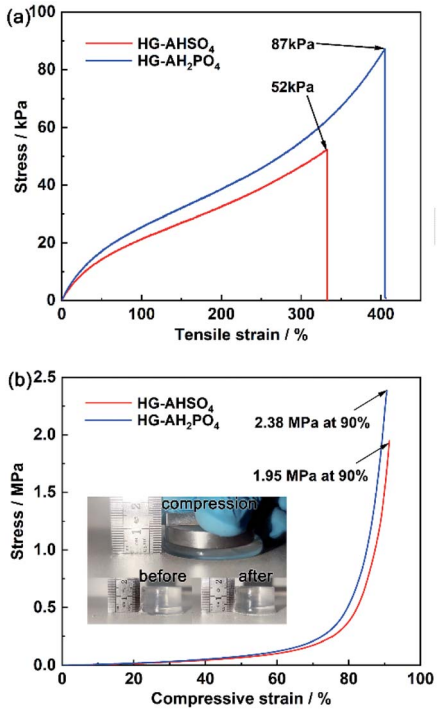

Fig. 6 (a) Tensile and (b) compressive stress–strain curves of HG-$AHSO_4$ and HG-AH_2PO_4 (insets are photographs of HG-AH_2PO_4 before and after compression).

4.3. Effect of anion on the thermal stability of the hydrogels

TG curves of HG-$AHSO_4$ and HG-AH_2PO_4 are shown in Fig. 7. The initial weight loss at temperatures below 200 °C was attributed to the dehydration. At higher temperatures, a two-step decomposition process was observed for the both hydrogels. For HG-$AHSO_4$, the first step decomposition began at 235 °C, arising from the breakdown of NH_4HSO_4.[23] In the case of HG-AH_2PO_4, the first step decomposition at 273 °C was ascribed to the breakdown of $NH_4H_2PO_4$.[24] The second step decompositions of HG-$AHSO_4$ and HG-AH_2PO_4 began at 364 °C and 429 °C, respectively. The weight loss in the second step was attributed to the degradation of the polymer network. Like PAM hydrogels derived from H_2SO_4 solution with different concentrations, PAM of HG-$AHSO_4$ exhibited a lower degradation temperature than that of HG-AH_2PO_4 because of lower pH level.[13] After the two-step decomposition, the residues of the hydrogels remained approximately 10 wt%.

4.4. Effect of anion on the ionic conductivities

Conductivities of HG-$AHSO_4$, HG-AH_2PO_4 and the aqueous solutions of NH_4HSO_4 (1.1 mol L^{-1}) and $NH_4H_2PO_4$ (1.1 mol L^{-1}) were obtained from EIS measurements. As shown in Fig. 8a, a typical impedance of the ammonium salt electrolytes consisted of an inclined line. An equivalent circuit containing two constant phase elements (CPE_1 and CPE_2) and the bulk resistance R_b was fit well to the impedance (inset of Fig. 8a). The ionic conductivities based on the derived R_b as functions of temperature are shown in Fig. 8b. The aqueous solution of NH_4HSO_4 exhibited a higher conductivity than that of $NH_4H_2PO_4$ at the same temperature owing to the higher H^+ concentration. Because the dissociation constant of the HSO_4^- anion (1.2×10^{-2}) was much higher than that of the $H_2PO_4^-$ anion (6.2×10^{-8}),[25] NH_4HSO_4 led to a lower pH level (0.75) than $NH_4H_2PO_4$ (3.96) after dissolved in water. At 30 °C, the aqueous solutions of NH_4HSO_4 and $NH_4H_2PO_4$ exhibited ionic conductivities of 360 and 104 mS cm^{-1}, respectively. Since the

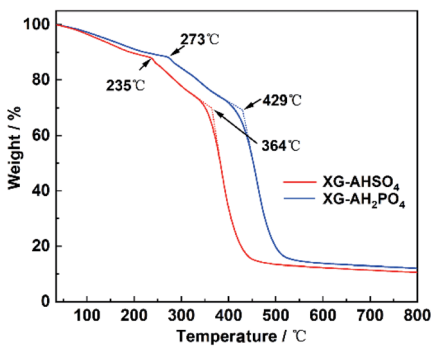

Fig. 7 TG curves of HG-$AHSO_4$ and HG-AH_2PO_4 obtained under an air atmosphere.

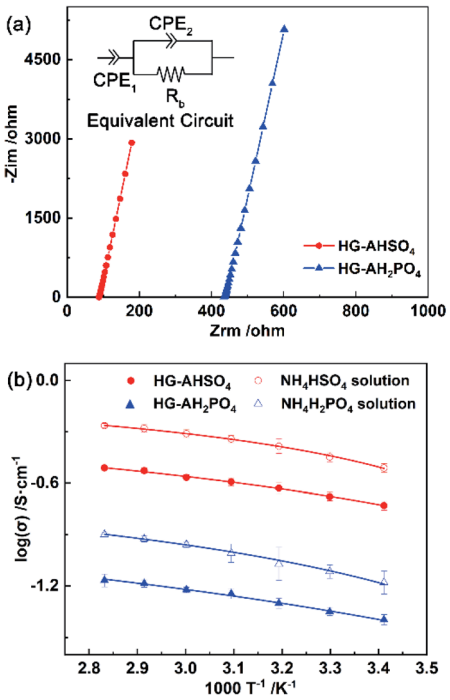

Fig. 8 (a) EIS spectra of HG-$AHSO_4$ and HG-AH_2PO_4 at 30 °C and (b) temperature dependence of conductivities for HG-$AHSO_4$, HG-AH_2PO_4 and the aqueous solutions of NH_4HSO_4 and $NH_4H_2PO_4$ (solid lines are fitting curves).

molar concentration of the two ammonium salts was identical, the higher ionic conductivity of the NH_4HSO_4 solution should be ascribed to more hydronium ions resulted from the anion dissociation.

Ionic conductivity of HG-$AHSO_4$ was also always higher than that of $NH_4H_2PO_4$ over the measured temperature range. Because partial acid anions formed hydrogen bonds with the amide group of PAM, pH values of HG-$AHSO_4$ and HG-AH_2PO_4 increased to 1.35 and 4.41, respectively. At 30 °C, ionic conductivity of HG-$AHSO_4$ reached 225 mS cm^{-1}, which was higher than that of the 3.5 mol L^{-1} H_2SO_4-doped PAM hydrogel (184 mS cm^{-1}).[13] Meanwhile, ionic conductivity of HG-AH_2PO_4 (46 mS cm^{-1}) was also superior to the 14.3 mol L^{-1} (85 wt%) H_3PO_4-doped PAM hydrogel (10 mS cm^{-1}).[11] The higher conductivities of the hydrogels doped with the mono-ammonium salts were attributed to the protonated ammonium cation, which can enhance proton conduction *via* both forming hydrogen bond and acting as proton carrier.[26] At 80 °C, ionic conductivities of HG-$AHSO_4$ and HG-AH_2PO_4 climbed to 309 and 65 mS cm^{-1}, respectively.

4.5. Activation energies for the ionic conduction

The temperature-dependent conductivities of the doped hydrogels were fit well to the Vogel–Tamman–Fulcher (VTF) equation.[27]

$$\sigma = \sigma_0 \exp\left[\frac{-E_a}{R(T - T_0)}\right] \quad (2)$$

Where σ_0, E_a, R, and T_0 are the pre-factor (S cm^{-1}), activation energy (kJ mol^{-1}), ideal gas constant (8.314 J mol^{-1} K^{-1}) and the Vogel temperature (K), respectively. According to the VTF behavior, it was speculated that the vehicle mechanism the ionic conduction in the hydrogels doped with the ammonium salts.[27] In this case, hydronium ions, the ammonium cation, and the acidic anions migrated to account for the observed conductivities.[28] The derived E_a values for the ionic conduction of HG-$AHSO_4$ and HG-AH_2PO_4 were 0.440 and 0.748 kJ mol^{-1}, respectively. In comparison with corresponding ammonium salt solution, E_a of the hydrogel approximately doubled owing probably to the hindrance of the polymer network to the conduction. The higher E_a of HG-AH_2PO_4 may be ascribed to larger volume of the $H_2PO_4^-$ anion, which was harder to diffuse in the hydrogels. The parameters resulted from the VTF fitting are listed in Table 1.

4.6. Fuel cell performance

HG-$AHSO_4$ and HG-AH_2PO_4 membranes with a thickness of 200 μm were assembled into fuel cells to evaluate the electrochemical performance under practical working conditions. The resultant polarization curves at 25 °C are shown in Fig. 9. The open-circuit voltages (OCV) of the fuel cells fabricated from HG-$AHSO_4$ and HG-AH_2PO_4 were 1.02 and 0.96 V, respectively. The higher OCV resulted from HG-$AHSO_4$ indicated that the smaller pores of the polymer network prevented hydrogen and oxygen from penetrating the membrane more efficiently. The short-circuit current (ISC) of the fuel cell fabricated from HG-$AHSO_4$ was much higher than that from HG-AH_2PO_4, in accordance with the results of the EIS characterization. A peak power density (P_{max}) of 106 mW cm^{-2} was achieved from HG-$AHSO_4$,

Table 1 Parameters resulted from the fitting to the VTF equation

Electrolytes	E_a/kJ mol^{-1}	σ_0/mS cm^{-1}	R^2
NH_4HSO_4 solution	0.216	360	0.998
$NH_4H_2PO_4$ solution	0.315	104	0.997
HG-$AHSO_4$	0.440	225	0.996
HG-AH_2PO_4	0.748	46	0.995

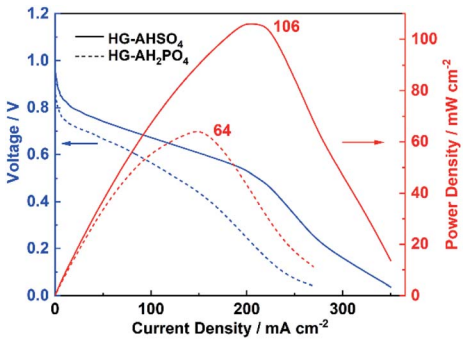

Fig. 9 Polarization curves of the H_2/O_2 fuel cells fabricated from HG-$AHSO_4$ and HG-AH_2PO_4 at 25 °C.

which overtook P_{max} obtained from the H_2SO_4-doped hydrogel with the same membrane thickness (74 mW cm^{-2}).[13] The result confirmed the advantage of ammonium salts over corresponding inorganic acids for proton conduction. A lower P_{max} (64 mW cm^{-2}) was obtained from HG-AH_2PO_4 due to the declined proton conductivity. The measured VOC, ISC and P_{max} for the fuel cells fabricated from HG-$AHSO_4$ and HG-AH_2PO_4 are summarized in Table 2.

Performance stability of the HG-$AHSO_4$ and HG-AH_2PO_4 fuel cells was evaluated by recording OCV at 25 °C with a certain interval (24 h).[29] As shown in Fig. 10, OCV of the fuel cell fabricated from HG-$AHSO_4$ kept relatively stable and maintained above 90% of its initial value for 1272 h. For HG-AH_2PO_4, OCV of the fuel cell decreased to 90% of its initial value in 744 h. The faster OCV attenuation of the fuel cell fabricated from HG-AH_2PO_4 was assumed to be related to the larger pores of the polymer network, which allowed easier penetration of fuel gas. The stability measurements suggested that the hydrogels doped with the ammonium salts were durable for long-term operation of the fuel cells.

Table 2 Performance of the fuel cells fabricated from HG-$AHSO_4$ and HG-AH_2PO_4 at 25 °C

Electrolytes	OCV/V	ISC/mA cm^{-2}	Peak power density/mW cm^{-2}
HG-$AHSO_4$	1.027 ± 0.011	350 ± 10	106 ± 3
HG-AH_2PO_4	0.960 ± 0.009	159 ± 8	64 ± 2

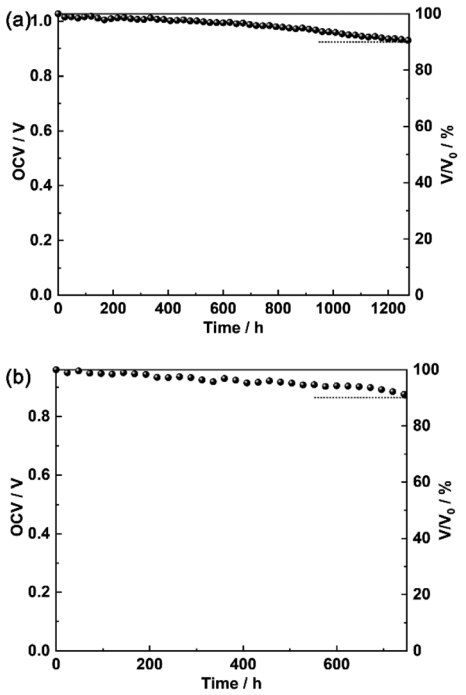

Fig. 10 Time-dependent OCVs of the fuels cells fabricated from (a) HG-$AHSO_4$ and (b) HG-AH_2PO_4.

5. Conclusions

The potential application of monoammonium salts of multiprotic acids as dopants to construct proton-conductive hydrogel membranes for fuel cell was demonstrated. Also, the effects of acid anions on thermal, mechanical, and electrochemical performance of the hydrogel membranes were evaluated. Robust hydrogel membranes were obtained by copolymerization of AM and EGDMA in aqueous solutions of NH_4HSO_4 and $NH_4H_2PO_4$. Conductivity of the hydrogel doped with NH_4HSO_4 was superior to that with $NH_4H_2PO_4$. Owing to the contribution of the protonated ammonium cation, the hydrogels doped with the ammonium salts exhibited higher conductivities than those doped with the corresponding inorganic acids. Performance tests of the fuel cells fabricated from the hydrogel membranes doped with NH_4HSO_4 and $NH_4H_2PO_4$ showed that the monoammonium salts of multiprotic acids can be used as suitable dopants to enhance proton conductivity of flexible electrolytes for electrochemical devices.

Conflicts of interest

The authors declare no competing financial interest.

Acknowledgements

This research did not receive any specific grant from funding agencies in the public, commercial, or not-for-profit sectors.

Notes and references

1 D. Y. Zhai, B. Liu, Y. Shi, L. J. Pan, Y. Q. Wang, W. B. Li, R. Zhang and G. H. Yu, *ACS Nano*, 2013, **7**, 3540–3546.
2 Q. Y. Chai, Y. Jiao and X. J. Yu, *Gels*, 2017, **3**, 6.
3 Y. Zhao, B. Liu, L. J. Pan and G. H. Yu, *Energy Environ. Sci.*, 2013, **6**, 2856.
4 Z. F. Wang, H. F. Li, Z. J. Tang, Z. X. Liu, Z. H. Ruan, L. T. Ma, Q. Yang, D. H. Wang and C. Y. Zhi, *Adv. Funct. Mater.*, 2018, **28**(48), 1804560.
5 M. K. Yazdi, V. Vatanpour, A. Taghizadeha, M. Taghizadeh, M. R. Ganjali, M. T. Munir, S. Habibzadeh, M. R. Saeb and M. Ghaedi, *Mater. Sci. Eng., C*, 2020, **114**, 111023.
6 C. Y. Chan, Z. Wang, H. Jia, P. F. Ng, L. Chow and B. Fei, *J. Mater. Chem. A*, 2021, **9**, 2043–2069.
7 M. Suzuki, T. Yoshida, S. Kobayashi, T. Koyama, M. Kimura, K. Hanabusa and H. Shirai, *Phys. Chem. Chem. Phys.*, 1999, **1**, 2749–2753.
8 E. Zygadło-Monikowska, Z. Florjańczyk, E. Wielgus-Barry and E. Hildebrand, *J. Power Sources*, 2006, **159**, 392–398.
9 Z. Gao, L. Kong, R. Jin, X. Liu, W. Hu and G. Gao, *J. Mater. Chem. C*, 2020, **8**, 11119.
10 N. Wen, B. Jiang, X. Wang, Z. Shang, D. Jiang, L. Zhang, C. Sun, Z. Wu, H. Yan, C. Liu and Z. Guo, *Chem. Rec.*, 2020, **20**, 773–792.
11 W. Wieczorek, Z. Fldrjanczyk and J. R. Stevens, *Electrochim. Acta*, 1995, **40**, 2327–2330.

12 J. Przyluski, Z. Poitarzewski and W. Wieczorek, *Polymer*, 1997, **39**, 4343–4347.
13 X. Wang, J. You and Y. Wu, *RSC Adv.*, 2021, **11**, 22461–22466.
14 A. Katzenberg, C. Muñoz Davila, B. Chen, T. Siboonruang and M. A. Modestino, *ACS Appl. Polym. Mater.*, 2020, **2**, 2046–2054.
15 K. P. Radha, S. Selvasekarapandian, S. Karthikeyan, M. Hema and C. Sanjeeviraja, *Ionics*, 2013, **19**, 1437–1447.
16 M. Kumar and S. S. Sekhon, *Eur. Polym. J.*, 2002, **38**, 1297–1304.
17 H. Pu and P. Huang, *Mater. Lett.*, 2006, **60**, 1724–1727.
18 S. Abdurrahmanoglu and O. Okay, *J. Macromol. Sci., Part A: Pure Appl.Chem.*, 2008, **45**, 769–775.
19 Y. Zhang, Y. Duan and T. Wang, *Phys. Chem. Chem. Phys.*, 2014, **16**, 26261.
20 F. B. Brahim and A. Bulou, *Mater. Chem. Phys.*, 2011, **130**, 24–32.
21 F. G. C. Tessarolli, S. T. S. Souza, A. S. Gomes and C. R. E. Mansur, *J. Appl. Polym. Sci.*, 2019, **136**, 47556.
22 G. Yu, C. Yang, N. Dan, W. Dan and Y. Chen, *Des. Monomers Polym.*, 2021, **24**, 293–304.
23 L. Mao, A. T-Raissi, C. Huang and N. Z. Muradov, *Int. J. Hydrogen Energy*, 2011, **36**, 5822–5827.
24 R. H. Chena, C. C. Yen and C. S. Shern, *J. Appl. Phys.*, 2005, **98**, 044104.
25 S. S. Zumdahl and S. A. Zumdahl, *Chemistry-Experimental Chemistry*, Houghton Mifflin Harcourt, 9th edn, 2014.
26 S. Miyazawa, R. Hosono, R. Osuga, J. Nomura Kondo and S. Uchida, *Acta Crystallogr., Sect. C: Struct. Chem.*, 2018, **74**, 1289–1294.
27 M. B. Karimi, F. Mohammadi and K. Hooshyari, *Phys. Chem. Chem. Phys.*, 2020, **22**, 2917–2929.
28 C. Ajith, A. P. Deshpande and S. Varughese, *J. Polym. Sci., Part B: Polym. Phys.*, 2016, **54**, 1087–1101.
29 S. Y. Lee, A. Ogawa, M. Kanno, H. Nakamoto, T. Yasuda and M. Watanabe, *J. Am. Chem. Soc.*, 2010, **132**, 9764–9773.